

PAPER

Correlation driven topological nodal ring ferromagnetic spin gapless semimetal: CsMnF₄

To cite this article: Anuroopa Behatha *et al* 2021 *J. Phys.: Condens. Matter* **33** 165803

View the [article online](#) for updates and enhancements.



IOP | ebooks™

Bringing together innovative digital publishing with leading authors from the global scientific community.

Start exploring the collection—download the first chapter of every title for free.

Correlation driven topological nodal ring ferromagnetic spin gapless semimetal: CsMnF₄

Anuroopa Behatha, Argha Jyoti Roy, C V Anusree, L Ponvijayakanthan, Vineet Kumar Sharma and V Kanchana*

Department of Physics, Indian Institute of Technology Hyderabad, Kandi—502285, Sangareddy, Telangana, India

E-mail: kanchana@iith.ac.in

Received 1 December 2020, revised 5 March 2021

Accepted for publication 18 March 2021

Published 20 April 2021



Abstract

The observation of in-plane ferromagnetism in layered magnetic materials in conjunction with the topological nodal-ring dispersion in a spin gapless semimetal with 100 % spin polarization has a fertile ground for novel physics, rich scientific significance and for the next-generation advanced spintronic and topological devices. Topological nodal ring spin gapless semimetals with large band gap in the other spin channel prevents the spin leakage and are excellent spintronic materials. On the basis of density functional theory (DFT), we have studied the layered magnetic perovskite, CsMnF₄ which is predicted to be a ferromagnetic insulator though the fellow compounds like AMnF₄ (A = Na, K, Rb) are anti-ferromagnetic in nature. DFT + *U* calculations reveal that this layered system undergoes a transition from an insulating to half-semimetallic nature with decreasing on-site Hubbard Coulomb interaction, *U*. For *U* = 2.5 eV, we observe the topological nature in the system with the emergence of four Mexican hat like dispersions associated with band-flipping. Also, we calculated the magneto-crystalline anisotropic energy with inclusion of spin-orbit coupling (SOC) and found that the system consists of in-plane ferromagnetism. Transport properties infer huge anisotropy of one order of magnitude between 'a' and 'c' axes. Interestingly, the estimated Fermi velocities are 2.66×10^5 and 2.24×10^5 m s⁻¹ for Z(=0) and Z(=0.5) plane respectively and are comparable to that of graphene, which might fetch applications in high speed spin electronic devices. The topological phase observed is robust to SOC and the band-crossings associated with nodal rings could be preserved by additional symmetry as the time-reversal symmetry breaks in magnetic systems. The nearly charge compensation observed from Fermi surfaces might fetch memory device applications.

Keywords: electronic structure, magnetism, nodal ring spin gapless semimetal

 Supplementary material for this article is available [online](#)

(Some figures may appear in colour only in the online journal)

1. Introduction

Topological materials (TM), are a fashionable and intriguing topic that not only grabs the focus of many researchers

by providing a platform in realising novel physics in condensed matter, but they also possess a rich scientific significance and broad application potential [1–13]. Some of these applications include novel quantum Hall effect [14], giant linear magnetoresistance [15] and so on. The presence of band crossings near the Fermi level in 3D materials is the

* Author to whom any correspondence should be addressed.

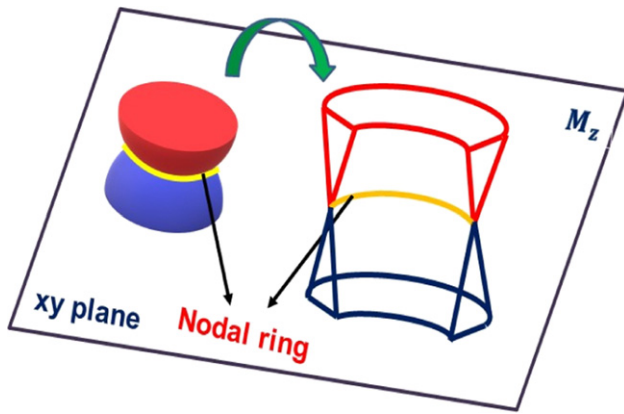


Figure 1. Schematic representation of a nodal ring in xy plane protected by a mirror reflection plane.

representative signatures of a TM. Depending upon the nature of the band crossings, the TM are classified into materials that host zero-dimensional (0D) nodal points or one-dimensional (1D) nodal line etc. If these nodal points/lines are associated with band crossings that are four-fold (two-fold) degenerate, they are described as Dirac (Weyl) nodal points/lines. For instance, in Dirac (Weyl) semimetals, this highly linear dispersive bands intersect at isolated points close to the Fermi level (E_F) and are considered to be nodal points. The electrons around this linear dispersion are described by the Dirac (Weyl) equation of the relativistic quantum field theory which allows the emergence of Dirac (Weyl) Fermions. Besides the 0D nodal points, band crossings in TM can also be continuous such as 1D nodal lines (NLs). If this nodal line circles around specific high-symmetric points in the Brillouin zone (BZ), we consider it to be a nodal ring. The schematic representation of an example of a nodal ring in the xy -plane protected by mirror symmetry is shown in figure 1. However the nodal points or NLs are further classified into two types (type1 & type2) based on the degree of tilting at the band crossing points. A recent study of the antiferromagnetic monolayer CrAs_2 , reports the coexistence of such type-1 & type-2 NLs [16].

An interesting classification among the TM is topological nodal line semimetals, where the lowest conduction band and highest valence bands touch each other along a 1D line close to the E_F . If this continuous band of touching points forms a closed loop around a high symmetry point in BZ, then the compound is termed as topological nodal ring semimetals. This new class of TM are extensively studied for their novel properties [17–25].

To date, topological properties have been extensively studied for non-magnetic compounds due to the appropriate presence of time-reversal (TRS) and inversion symmetry. But the story changes, due to the breaking of time reversal symmetry (TRS) in magnetic systems, and the nodal points or NL are required to be protected by additional symmetries. Hence examples of magnetic TM [18] are comparatively less. Few such studies on magnetic systems include single crystal Weyl semimetal candidates like pyrochlore iridates [26]

& HgCr_2Se_4 [27], CuMnAs [28] Co-based Huesler alloys [16, 29, 30] etc.

Also NLs/rings present in the system need not be fully spin-polarized. It would be interesting to have a system with a wide band gap in one spin channel so that they are resistant to thermally induced spin-flip transitions at room temperature. Recently, a new class of materials (i.e., spin gapless semiconductors) have been identified which are considered to be an upgraded version of the existing half-metals because of their high electron mobilities and other interesting properties [31]. Such spin gapless semimetals (SGSs) hosting topological NLs, with 100 % spin polarization associated with large band gaps in another spin channel combine spintronics and topology together and find application in advanced spintronic devices. Such candidates are considered to be topological nodal line spin gapless semimetals and exhibit ultra high Fermi velocities [32, 33]. Recent findings of intrinsic ferromagnetism along with topological properties in a two-dimensional rhenium halide paved a way for potential realization of the quantum Hall effect [34]. Interestingly, in this compound, the DFT + U calculations reveals the transition from a non-trivial to trivial state with increasing on-site Hubbard Coulomb interaction U through the emergence of a Dirac cone which is corroborated by the emergence of chiral edge states and anomalous Hall conductivity. Such studies motivated us to work on the well known layered magnetic perovskite, CsMnF_4 which is predicted to be a ferromagnetic insulator [35].

CsMnF_4 crystallizes in tetragonal structure with the space group $P4/nmm$ [35] same as that of CsFeF_4 , although the magnetic structure of these are not the same with the latter being antiferromagnetic [36]. CsMnF_4 is reported to be a 2D ferromagnetic insulator which is quite rare. The compound has similar structure to that of TlAlF_4 [37]. The x-ray diffraction studies by Massa *et al* reveals CsMnF_4 to have a puckered layered structure [35]. Neutron diffraction experiments showed that the compound has planar magnetization and a magnetic moment $\mu_B = 4.04 \pm 0.2$ [38]. The magnetic susceptibility measured using SQUID and Foner magnetometers confirmed the ferromagnetic nature of the solid and the evaluated value of exchange energy J/k is found to be +1.30 K [39] which also explains the relatively low T_c and weak ferromagnetism. CsMnF_4 is one member of the family of layered fluorides AMnF_4 ($A = \text{K, Rb, Cs}$). Of these, only the Cs compound is ferromagnetic with the experimentally reported Curie temperature of $T_c = 18.9\text{K}$ while the K and Rb derivatives are antiferromagnetically ordered at 3.7 and 5.2 K respectively [38]. Pressure dependent structure studies on CsMnF_4 reveal the system to undergo a structural phase transition to the orthorhombic RbMnF_4 structure (space group $Pmab$) at around 1.5 GPa and this is expected to have antiferromagnetic ordering below T_c ([38]). The high pressure optical absorption spectroscopy study conducted by Aguado *et al* on CsMnF_4 shows that this exhibits a spin crossover from high spin $S = 2$ to low spin $S = 1$ configuration due to Jahn Teller suppression at 37 GPa. The low spin state is found to be stable up to 46 GPa, and when the pressure was released, an abrupt reversible change was observed at 30 GPa to the high spin state. This simultaneous spin change and Jahn–Teller

suppression involves a first order structural phase transition [40].

In the present work, we study the variation of electronic properties of CsMnF_4 as a function of Hubbard, U . At $U = 2.5$ eV, we observed that, CsMnF_4 turns out to be a ferromagnetic topological nodal ring SGS with 100% spin polarization.

This paper is organised as follows. In section 2, we discuss the computational methods used to study the present compound. Section 3 is devoted for the results and discussion which focuses on the magnetic, electronic, transport and topological properties of CsMnF_4 and last but not the least, we conclude our results in section 4.

2. Computational details

We have performed the first principle calculations using the accurate projected augmented planewave (PAW) [41, 42] method as implemented in Vienna *ab initio* simulation package (VASP) [42, 43] with a large plane-wave energy cut off of 520 eV for plane wave basis. In order to treat the exchange correlation effects, we have used generalised gradient approximation (GGA) method within the parametrization of Perdew–Burke–Ernzerhof parametrization (PBE) [44]. The valence configurations used throughout the calculations were $4s^2 3d^5$, $5s^2 5p^6 6s^1$ & $2s^2 2p^5$ for Mn, Cs and F respectively. A k -mesh sampling of $6 \times 6 \times 8$ has been used in the irreducible BZ. In order to achieve the ground state energy, the atomic positions along with the lattice parameters were relaxed using conjugate-gradient algorithm with the atomic force tolerance of 0.01 eV \AA^{-1} and total energy tolerance of 10^{-6} eV. For the better description of the 3d electrons, we have included GGA + U scheme [45] with a Hubbard U -value of 3.5 eV for Mn. Also the fully relativistic PAW potentials were used in order to include spin–orbit coupling (SOC) in the present system.

We have employed the semi-classical Boltzmann theory using BoltzTrap code [46] in order to compute the electrical conductivity scaled by relaxation time within constant relaxation time approximation and rigid band approximation (RBA). We have performed the surface studies using maximally localized Wannier functions (MLWFs) [47], in order to analyze the topological nature. At first, we have constructed the tight binding Hamiltonian using MLWFs in conjunction with VASP code. Further, the tight binding parameters are fed to WannierTools [48] package, which employs an iterative Greens function [49] technique for obtaining the surface state properties.

3. Results and discussion

3.1. Structural details, chemical bonding and stability

CsMnF_4 , a well known layered-perovskite, crystallizes in tetragonal structure with a space group P_4/nmm (129). It consists of $[\text{MnF}_6]$ octahedra which form a planar network and two such layers are separated by Cs atoms as illustrated in

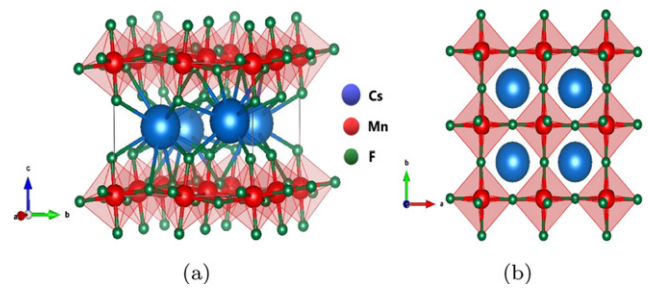


Figure 2. Representation of the crystal structure of CsMnF_4 with unit cell in (a), along 001 projection in (b) respectively.

Table 1. Experimental and calculated lattice parameters (in \AA) of CsMnF_4 in the ground state configuration (FM) as a function of Hubbard, U .

	a (\AA)	b (\AA)
Expt [35]	7.944	6.338
GGA	7.990	6.500
	GGA+ U (U in eV)	
$U = 2$	8.049	6.444
$U = 2.5$	8.055	6.427
$U = 3$	8.057	6.423
$U = 3.5$	8.065	6.427
$U = 4$	8.059	6.431

figure 2. The MnF_6 group deviates from being a proper octahedra due to the presence of Jahn–Teller active Mn^{+3} cation. The experimental lattice parameters (i.e., $a = 7.9440 \text{ \AA}$ & $c = 6.3376 \text{ \AA}$) along with their positions are reported by Massa *et al* [35]. We have performed the optimization of geometry and internal structural parameters within both the GGA and GGA + U schemes. Experimental and theoretical lattice constants are given in table 1 and are in reasonable accordance with each other.

In order to understand the chemical bonding in CsMnF_4 , we have plotted the charge density distribution along (100) and (110) planes (see figure 3). Fluorine (F), being the most electronegative element, receives the electrons from Cs and Mn (i.e., the flow of charge would be towards F). However in (110) plane (see figure 3 (right)), we observe the sharing of charge between transition metal (Mn) and halide atoms (F). This reflects the covalent nature of bonding between Mn and F which is mainly due to the hybridisation of Mn– d and F– p states. This nature is very well observed in partial density of states (DOS), which highlights the strong hybridisation between Mn– d and F– p states near the Fermi level and the spherical charge distribution around Cs atom reflects the ionic bonding between Cs and MnF_6 . From the figure 3 (left) (i.e., in 100 plane), we observe that the charge flow occurs only within the layers but not out of these. This reflects the anisotropic nature of the system. In order to explain the structural stability of this compound, we have computed the cohesive energy/atom. The negative energy values confirm that the system is bound and stable (see table 1 in supporting information (<https://stacks.iop.org/JPCM/33/165803/mmedia>) (SI)).

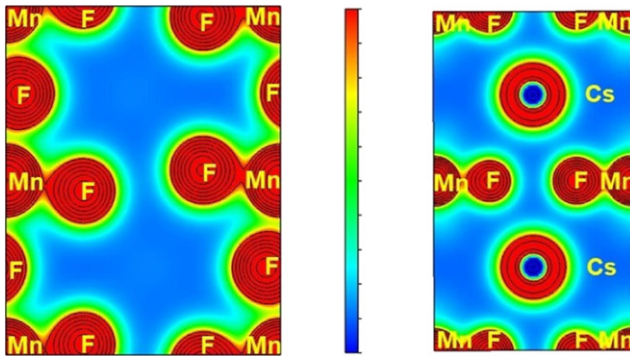


Figure 3. Charge density distribution plots of CsMnF₄ along (100) plane which highlights that the charge flow is purely in *xy* plane but not along *z* direction (left) and (110) showing the ionic bonding between Cs and MnF₆ and covalent bonding between Mn and F atoms (right).

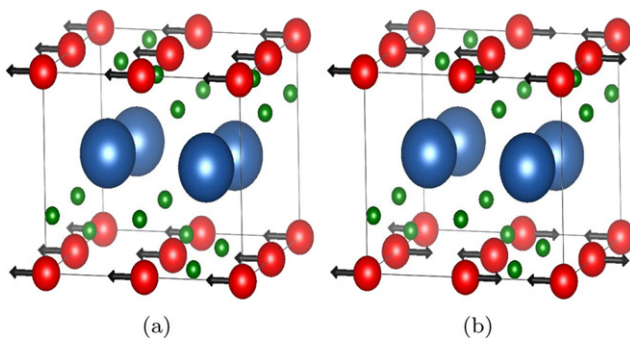


Figure 4. Crystal structure with two magnetic configuration (a) FM (b) AFM1.

3.2. Magnetic properties

In compounds like CsMnF₄, magnetism is due to the presence of unpaired spins on the transition-metal element. The octahedral environment around Mn splits the 3d orbital into t_{2g} and e_g states, with t_{2g} at lower energy. The four 3d electrons generally remains in high spin state with $S = 2$ and our calculations reflect the same which will be discussed further.

In order to understand the ground state magnetism in this compound, we have optimised the structure and compared the energies in two possible magnetic configurations (i.e., FM and AFM1 as shown in figure 4). Using the GGA XC-functional under PBE parametrisation, we could not find the FM configuration to be the stable state which is contrary to the experimental work [35]. To determine the proper ground state of a strongly correlated system like CsMnF₄, we proceeded the optimisation with GGA + U which includes the on-site repulsion by the Hubbard U value. We have considered U values from $U = 2$ to 4 eV with equal intervals of 0.5 eV. We have also calculated the magnetic anisotropic energy by including SOC with spin moments along the x and z directions and found that the easy axis is along x direction. The calculated energies (with SOC along the x & z direction) and the bond lengths, the planar angle details are shown in table 2 and the individual magnetic moment values of Mn as a function of U are given in table 3.

From our results, one can observe that, the ground state remains to be FM for all the investigated U values. Interestingly, the total magnetic moment remains an integer (i.e., $4 \mu_B$ per f.u.) for all values of U . Though the Hubbard U acts like a strain to the system this behaviour is expected as the compound has a spin transition only at very high pressure [40].

Ferromagnetic semiconductors are often discussed in terms of a competition between short range antiferromagnetic superexchange interaction and long-range carrier mediated mechanism establishing ferromagnetic order [50]. Here we use the semi empirical Goodenough–Kanamori–Anderson (GKA) [51–54] rules in explaining the ferromagnetic state of our compound. The sign and magnitude of the superexchange interaction between the magnetic cations depends on (i) cation–anion–cation bond angle (ii) oxidation state of the magnetic cation (i.e., no of d electrons present) and (iii) symmetry of the crystal field. Though, the magnitude of the superexchange requires a downfolding procedure as implemented in NMTO code [55], the sign of the interaction can be established using the GKA rules. The interaction between half-filled cation orbitals leads to antiferromagnetic coupling, whereas the interaction of one half filled and empty orbital of the cation exhibits ferromagnetic coupling. This exchange interaction can be regarded as kinetic exchange between the atoms participating and a potential exchange between the orthogonal orbitals which are always ferromagnetic [56]. It should be noted that the sign of kinetic exchange depends on the filling of the transition metal d orbital.

In an octahedral environment, the five fold degenerate ‘ d ’ orbitals split into doubly degenerate e_g and triply degenerate t_{2g} levels. The compressed octahedral environment further splits the e_g and t_{2g} levels. The crystal field splitting (i.e., $\Delta = 1.36$ eV) and the energy splittings of each e_g and t_{2g} levels are 0.18 and 0.08 eV respectively which are shown in figure 5. The bond angle Mn–F–Mn is closer to 180-degree with Mn⁺³ (d^4) state as in figure 5. It is important to note that 180-degree superexchange are antiferromagnetic in nature but d^4 – d^4 configuration is bit tricky, the type of superexchange exhibited in d^4 – d^4 configuration depends on the line of superexchange [53]. Keeping all these in mind, we propose ferromagnetic superexchange pathway for our compound to be $d_{x^2-y^2} - p_x - d_{z^2}$ (see figure 5).

3.3. Electronic properties

We have carried out spin-polarised calculations under GGA approximation to perceive the ferromagnetic insulating nature as experimentally observed [35]. The details of the electronic ground state properties along with the partial DOS is given in SI (see figure 1). From the results, we observe the system to possess the half-metallicity, with conducting spin-up channel (up) and insulating spin-down channel (dn). The spin polarized DOS highlights the dominating nature of Mn– d and F– p states near E_F . As our calculations did not initially give the FM insulating nature, we continued our calculations by including onsite electronic correlations (i.e., GGA + U scheme [45]) for better description of the ground state properties.

Table 2. Calculated total energies for CsMnF₄ in different magnetic configurations. As an example, E_{FM}^x denotes the energy per formula unit for the FM state with spins aligned in x -direction. The ground state energy is taken to be zero (as a reference point).

U (eV)	Mn–F(Å) in plane	Mn–F(Å) out of plane	$\langle \text{Mn–F–Mn} \rangle$ in degrees	E_{FM}^x (meV)	E_{AFM}^x (meV)	E_{FM}^z (meV)	E_{AFM}^z (meV)
2	2.035	1.849	162.62	0	40.5	3.1	44.3
2.5	2.040	1.846	161.28	0	14.3	3.4	18.1
3	2.047	1.845	159.35	0	15.1	3.5	18.9
3.5	2.048	1.847	159.74	0	19.6	3.5	23.3
4	2.048	1.848	159.16	0	21.6	3.5	25.3

Table 3. Magnetic moments of Mn as a function of U .

	$U = 2$ eV		$U = 2.5$ eV		$U = 3$ eV		$U = 3.5$ eV		$U = 4$ eV	
	Orbital	Spin	Orbital	Spin	Orbital	Spin	Orbital	Spin	Orbital	Spin
GGA + U	—	3.798	—	3.809	—	3.823	—	3.845	—	3.866
GGA + U + SO	−0.024	3.794	−0.026	3.805	−0.027	3.818	−0.028	3.841	−0.029	3.862

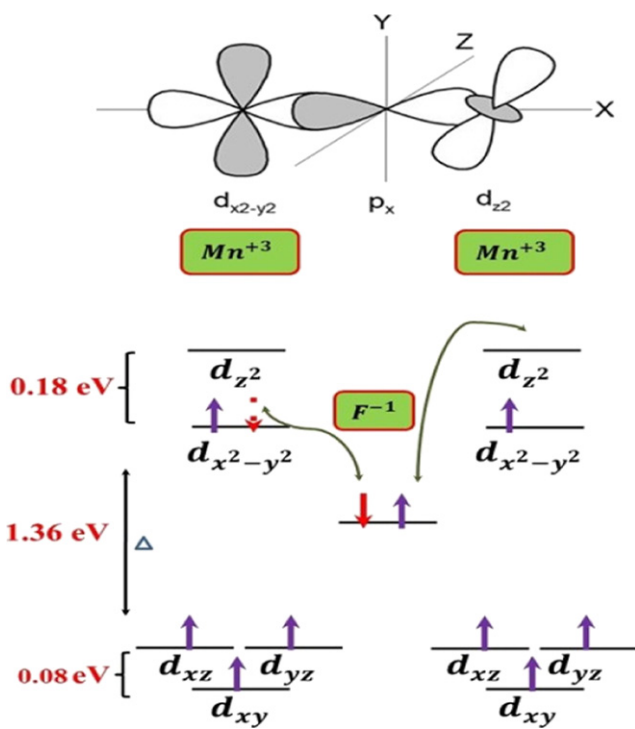


Figure 5. Schematic model of superexchange interaction between Mn and F ions leading to FM order in the structure.

We have performed a series of GGA + U calculations by varying U from 2 to 4 eV (i.e., $U = 2, 2.5, 3, 3.5, 4$ eV respectively). The ground state configuration (i.e., an FM insulating state) is achieved by applying Hubbard U value of 3.5 eV. At this U value, we obtain the semiconducting nature in one channel (up) and insulating nature in the other channel (down) with a band gap of 0.19 eV and 5.14 eV respectively as shown in figures 6(a) and (b). The spin-polarized DOS given in figure 5 (in SI) showcases the dominant nature of Mn- d and F- p states near E_F . In addition, we provide the orbital resolved bands structure of spin up channel in a view of analysing the atomic

orbital contributions at E_F . From the figure 7(a), we see that the conduction band is mainly from the Mn- d_{z^2} hybridized with F- p_z and valence band contribution arises from Mn- $d_{x^2-y^2}$ mostly which is hybridised with F- p_x, p_y . Among the Mn orbitals, unoccupied Mn- d_{z^2} in both spin up and spin down channel and partially occupied Mn- t_{2g} and $d_{x^2-y^2}$ (of e_g state) reflects the +3 oxidation state of Mn (i.e., Mn⁺³).

The similar orbital character and electronic property is found for the $U = 4$ eV (i.e., GGA + U calculation) with only change that, the band gap increases with increase in U . The details of electronic and magnetic properties are given in SI (see figure 6).

Interestingly we found that, electronic property changes with the variation of on-site electronic correlation effect (i.e., by varying Hubbard U -value in GGA + U calculations). As we decrease the Hubbard U from 3.5 eV to 3eV, the band gap decreases further and highlights the semi-metallic nature in one spin direction (up) and insulating nature in other direction (down) with corresponding pseudo gap in partial DOS. The electronic band structure along with the spin-polarized DOS are given in SI (see figure 4). The orbital contribution remains to be same as that of $U = 3.5$ eV case. However, when we further decrease U value from 3 to 2.5 eV, the system is driven to spin-semimetallic nature with one spin channel (up) conducting and other (down) insulating with a large band gap of around 4.6 eV. These changes in electronic property as a function of correlation, (i.e., U) prompted us to further investigate the system from various perspectives.

Surprisingly, we observe that there exists a quantum topological transition associated with character band flipping taking place from $U = 3.5$ to 2.5 eV. Figures 7(a)–(c) shows the orbital resolved spin up band structure along with corresponding 3d bands along the high symmetry path of Γ -X-M- Γ in figures 7(d)–(f) respectively. This figure clearly spotlights the character band-flipping on decreasing Hubbard U . Thus we

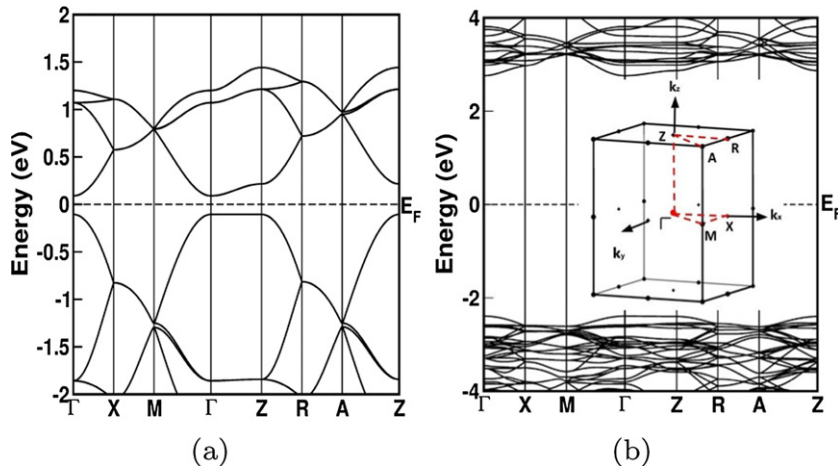
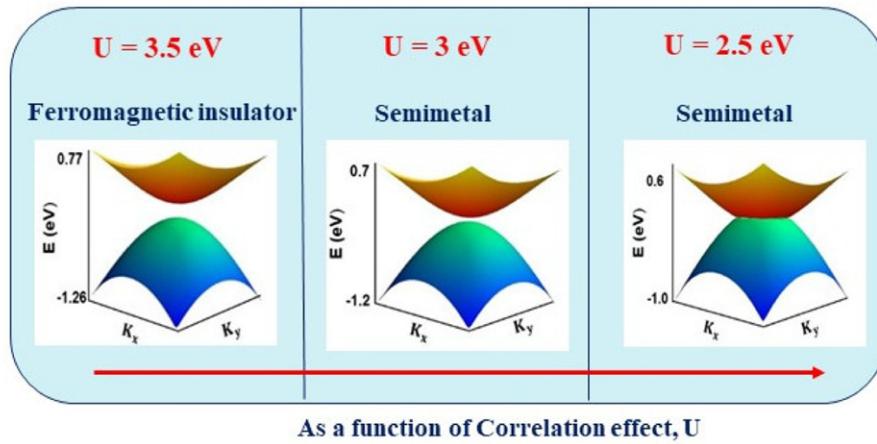
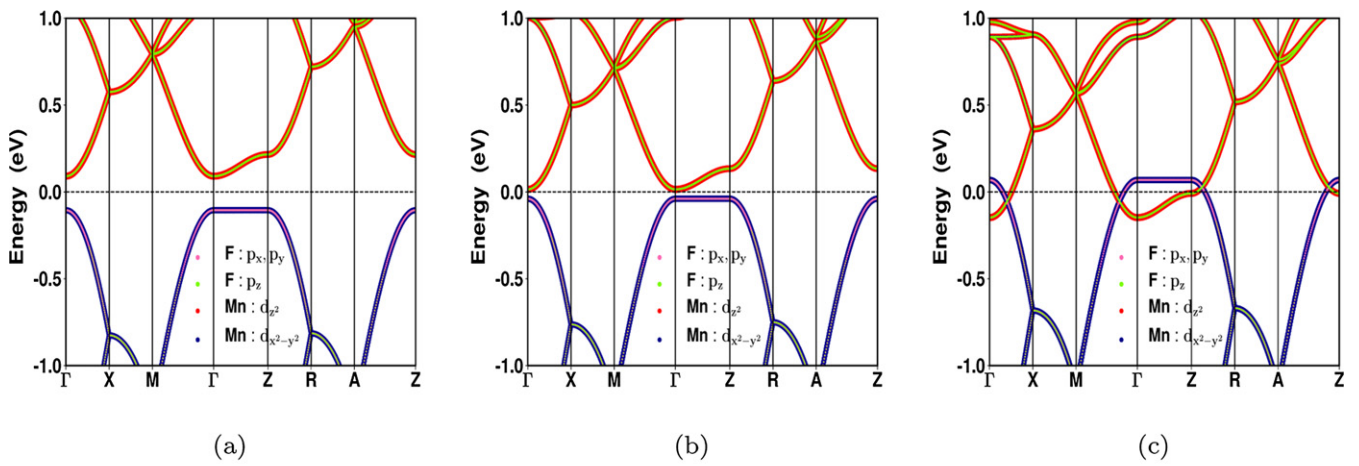


Figure 6. (a) and (b) Ground state electronic band structure reflecting the ferromagnetic insulating nature with spin up & spin down channels in $U = 3.5$ eV.



(d)

Figure 7. (a–c) Projected band structure of CsMnF₄ for $U = 3.5, 3, 2.5$ eV respectively and showing orbital character flip of d_{z^2} (p_z) and $d_{x^2-y^2}$ (p_x, p_y) by varying U . (d) Shows the corresponding 3D band structures.

capture the topological nodal line semimetal as a function of correlation effect and the details are further explained below.

Figure 8 highlights the spin-polarized electronic band structure, corresponding Fermi surfaces and transport properties in spin up direction at $U = 2.5$ eV. The details of the band

structure (spin down) and DOS is given in SI (see figures 3(a) and (b)). In spin up channel (figure 8(a)), the conduction band minimum and valence band maximum touches at two sets of iso-energy points along $\Gamma-X-M-\Gamma$ (below E_F) and $Z-R-A-Z$ (above E_F) leading to the Mexican hat like

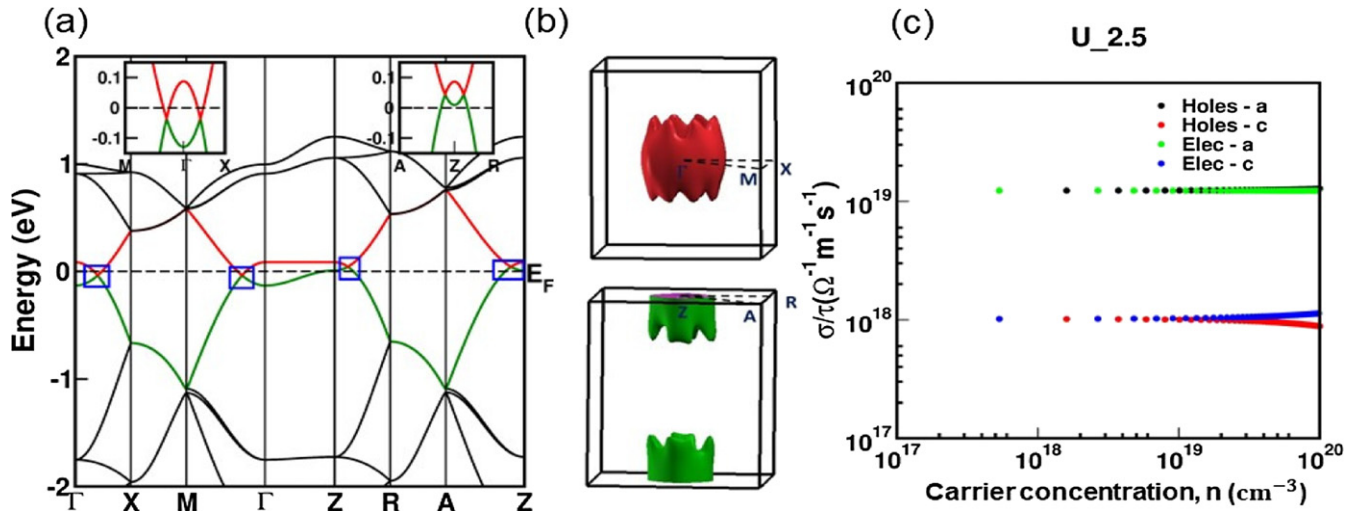


Figure 8. (a) Electronic band structure of spin up channel in $U = 2.5$ eV along with four unusual Mexican hat like dispersions shown in insets along the high symmetry path $M-\Gamma-X$ in BZ shown as an inset (b) Fermi surfaces representing hole and electron nature respectively. (c) Electrical conductivity scaled by relaxation time for $CsMnF_4$ at 400 K.

dispersions [57] around Γ and Z . The four unusual Mexican hat like dispersions (i.e., two from conduction bands and two from valence bands), which are shown in the insets of figure 8 hints for the possibility of nodal rings present in the system. Thus two nodal rings are expected around Γ and Z (i.e., NL1 and NL2).

To understand the electron and hole-like nature of bands, we have calculated the Fermi surface for $U = 2.5$ eV. The Fermi surface plots are shown in figure 8(b). The open cylinder Fermi surface, centered around Γ in $Z(=0)$ plane, corresponds to the red color band. This reflects the hole nature and the other one along $Z(=0.5)$ plane corresponds to the green color band. This is also a cylinder around high symmetry point Z , reflecting the electron nature. From these Fermi surface contours, it is predicted that the charge compensation will occur. An earlier study on charge compensation through the Fermi surface, claimed the possibility of high magneto-resistance and open Fermi surface leading to non-saturated magneto-resistance [58]. Other studies revealed the possibility of giant magneto-resistance through full charge compensation [58–61]. The observation of a nearly charge compensated Fermi surface in $CsMnF_4$ might lead to finite magneto-resistance possible memory device applications.

Figure 9 shows the orbital resolved band structure of $CsMnF_4$. Interestingly, there exists a band flipping of $Mn-d_{x^2-y^2}$, $F-p_x, p_y$ states with $Mn-d_{z^2}$, $F-p_z$ states in $U = 2.5$ eV which hints for the topological nature in this system. Zhang *et al* and Wang *et al* showed similar band character flip and highlighted the topological nature in their works [16, 62]. The 3D band structure, highlighting Mexican hat like dispersions, is shown in left (right) inset along the path $M-\Gamma-X$ ($A-Z-R$) (see figure 9). This gives the hint for the shape of the NL1 and NL2 which are circulating around Γ and Z respectively. However, the radius of the nodal ring, NL2 is less compared to that of NL1. Thus, four such unusual Mexican hat like band dispersions in $U = 2.5$ eV present along

the paths $\Gamma-X-M-\Gamma$ and $Z-R-A-Z$ (i.e., two from conduction bands and two from valence bands) demonstrates $CsMnF_4$ to be a topological nodal ring semimetal in spin up channel whereas spin down channel remains to be insulating. Since these nodal rings are found to be only due to one spin channel, it is believed to host great advantages in spintronic applications. Quite recently, He and Zhang *et al* showed similar spin-polarized nodal line study in an antiferromagnetic material $\beta-Fe_2PO_5$ [63].

We also performed SOC with magnetic moments aligned in the x -direction. Figure 3(a) in SI, shows that there exists no change in electronic properties when SOC is included and this is not surprising because of the fact that the Mn orbitals are half-filled at the Fermi level.

To get more details about the topological nature, we have proceeded with the surface state study along (001) surface using wannier functions. Figure 10(a) gives the schematic representation of nodal rings (in blue color) in (001) projected planes within the BZ, i.e., one around Γ and other around Z . The two nodal rings appear in (001) projected surface but with different radius which can be observed from the surface bands along (001) plane as shown in figure 10(b). A pair of iso-energy nodal rings (i.e., one around Γ and other around Z) along with the surface states are labeled in figure 10(b) with an inset along different path $\bar{M}-\bar{\Gamma}-\bar{X}$. The surface band structure also possesses the Mexican hat like dispersion as shown in the bulk and Fermi arc displays the two circular nodal rings (see figure 10(c)) as $CsMnF_4$ is ferromagnetic in nature, the TRS is broken and hence nodal rings are expected to be protected by additional symmetries. In our case, the investigated system possess the inversion, D_{4h} (4-fold rotational symmetry) and the nodal points present along the high symmetry path $\Gamma-M$, $\Gamma-X$ in $k_z = 0$ and $Z-R$, $Z-A$ in $k_z = \pi$ plane are protected by the glide mirror symmetry perpendicular to the (001) surface, thereby protecting the nodal rings (NL1 and NL2). Such symmetry protected NLs were discussed in earlier works for different materials [64–66]. All these above mentioned

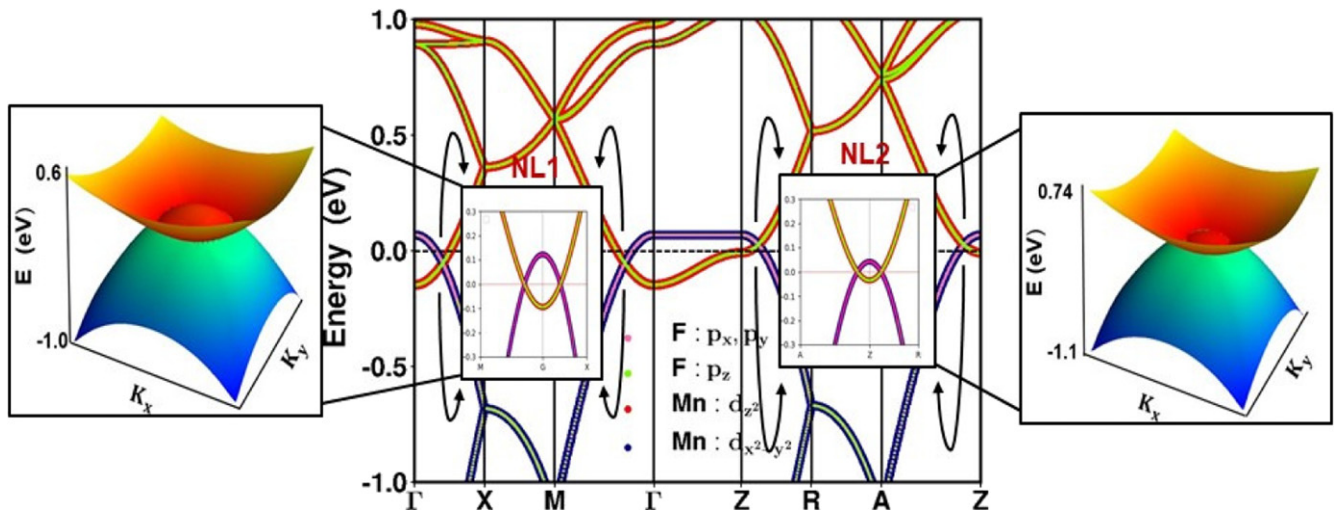


Figure 9. The bulk electronic band structure of CsMnF₄ with GGA + U ($U = 2.5$ eV) under PBE parametrization. The representation of Mexican hat like bands around Γ (Z) are indicated in insets along $M-\Gamma-X$ ($A-Z-R$). The orbital-projected band structures shows that the band near the Fermi level is mostly composed of Mn- d and F- p orbitals. The 3D band structure highlights the existence of nodal ring around Γ (Z) in $k_z = 0$ ($k_z = \pi$) plane.

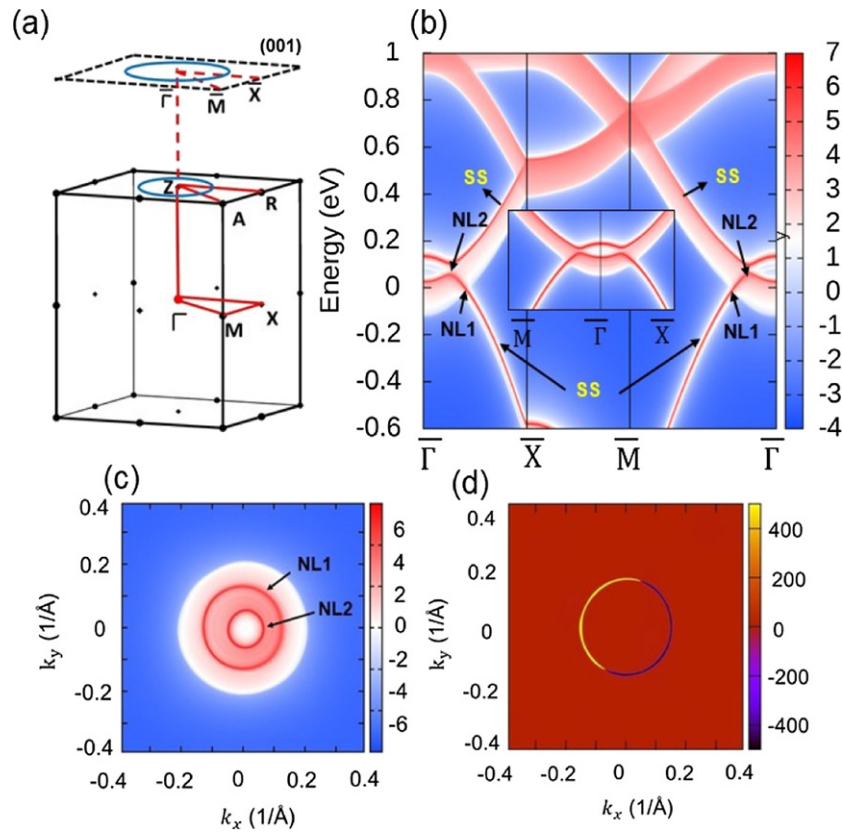


Figure 10. (a) Schematic representation of nodal rings, NL1 (NL2) around Γ (Z) in 001 plane (b) surface band structure plotted along 001 plane with an inset showing the Mexican hat like surface states (c) Fermi arc showing nodal rings (NL1 and NL2) along 001 plane. (d) Berry curvature, Ω_z in $k_z = 0$ plane.

interesting features demonstrate this system to be a topological nodal ring half-semimetal which can fetch application in spintronic devices. To get more insight about topological nature, we have calculated berry curvature and chern number as shown in figure 10(d) in $k_z = 0$ plane. The close contour suggests the

Berry curvature to be zero for this plane and the chern number, which is the integration of berry curvature over BZ will be zero inferring the trivial nature and claims the surface states to be trivial surface states. Another important parameter, Berry phase, which is the surface integral of Berry curvature also vanishes

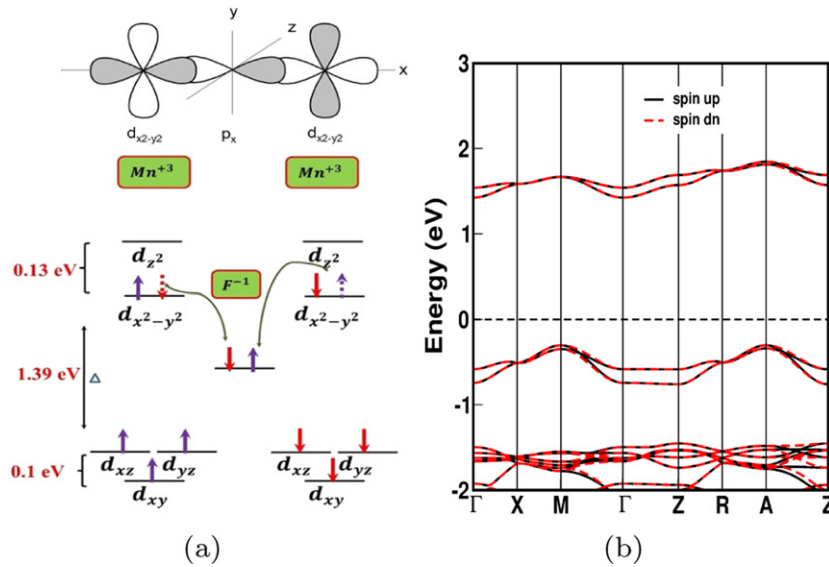


Figure 11. (a) Schematic model of superexchange interaction between Mn atoms via F atoms showing the AFM possibility in the system (b) electronic band structure at high pressure.

in $k_z = 0$ plane. Hence, we infer that, the investigated system possesses trivial topological nature. The electronic properties and physical properties remains same for $U = 2$ and 2.5 eV. Hence, the details of electronic properties of $U = 2$ eV is not shown here (see figure 2 in SI).

Prompted by the emergence of nodal rings near the Fermi level, we have analysed some transport characteristics for the $U = 2.5$ case. We can expect the Fermi velocity (v_F) to be much higher near the nodal rings, due to linear dispersion of the bands. So we have calculated the v_F through linear fitting using the relation $v_F = (1/\hbar) \cdot dE/dk$, which is valid for bands having non-parabolic dispersion [67]. Our estimated Fermi velocities are 2.66×10^5 and 2.24×10^5 m s⁻¹ for $Z(=0)$ and $Z(=0.5)$ plane respectively. The values of v_F are in the range of several well known Weyl semi-metals [68–70] and comparable to that of graphene, which indicates that CsMnF₄ may have application in high mobility transport. Further, we have calculated the electrical conductivity scaled by relaxation time (σ/τ) which is shown in the figure 8(c), for the crystallographic directions 'a' and 'c'. There is a huge anisotropy with nearly an order of magnitude difference between the 'a' and 'c' direction due to the linearly dispersive bands along the 'a' when compared to the 'c' direction which has flat band-dispersion.

Also, we have calculated the electrical conductivity for different U values as a function of temperature by fixing the carrier concentration at 10^{18} cm⁻³ and the details are given in the SI (figure 8). The investigated system shows metallic nature for the U values of 2 and 2.5 eV. As the CSTA and RBA fails to explain the correct nature of electrical conductivity with respect to temperature for metallic systems, we have performed the calculations for other U values (i.e. $U = 3, 3.5$ and 4 eV). It is observed that, the electrical conductivity increases with temperature and decreases as the Hubbard U value increases, which can be inferred from the electronic bandstructure as well.

4. Pressure study

CsMnF₄ being a weak ferromagnetic in nature, there arises the possibility for the occurrence of structural/magnetic phase transition under application of pressure and we found that, there exists the magnetic phase transition from FM to AFM at a pressure of 2.4 GPa. The driving force from FM to AFM transition is mainly due to the decrease in superexchange angle within the layers (i.e., Mn–F–Mn angle). A critical superexchange angle, $\alpha_c = 156.7^\circ$ is determined from our theoretical study. However the experimentally reported [38] value is 147° . This change can be attributed to the variation of experimental and theoretically obtained parameters. The reduction in superexchange angle is due to the decrease in volume of the cell. As the volume decreases, the bond lengths between Mn–F changes, the distance between the adjacent layers decreases thereby octahedra within the layers get affected due to the change in electronic forces which causes this dramatic change from the magnetic point of view (i.e., FM to AFM transition). The variation in bond lengths and bond angle from the ground state FM to AFM state is given in SI (see figure 7(a)). The schematic model explaining the AFM state possibility is shown in figure 11(a).

The details of electronic properties of CsMnF₄ after the transition pressure are given in figure 11(b), spin-polarized DOS are given in figure 7(b) in SI, which reflects the anti-ferromagnetic insulating nature with and indirect band gap of 2 eV.

5. Conclusion

In summary, based on first-principles study, we analyzed the electronic, magnetic, transport and topological properties of a layered perovskite structure CsMnF₄. Hubbard U correlations are included in the system to well explain the ground state properties. We found that our system is ferromagnetic

insulating in nature with inclusion of U_{eff} value of 3.5 eV. However, the electronic band profile changes with the variation of U . At $U = 2.5$ eV, we observed two nodal rings associated with four unusual Mexican hat like dispersions and band-flipping. Also, we have calculated the magnetocrystalline anisotropic energy with inclusion of SOC and found that the system consists of in-plane ferromagnetism with half- semi-metallicity. Observation of in-plane ferromagnetism along with topological phase in a SGS (100 % spin polarization) and a large band gap in other spin channel spotlights CsMnF₄ to be a topological nodal ring spin gapless semimetals. The observed topological phase is robust to SOC and the nodal rings are preserved by glide mirror symmetry as the time-reversal symmetry breaks in magnetic systems. Our estimated Fermi velocities, 2.66×10^5 and 2.24×10^5 m s⁻¹ for $Z(=0)$ and $Z(=0.5)$ plane respectively are comparable to that of graphene which might fetch high speed spin electronic devices. The observation of a nearly charge compensated Fermi surfaces in CsMnF₄ might lead to finite magnetoresistance possible memory device applications.

Acknowledgments

The authors AB, AJR, ACV, LP, VKS, VK would like to acknowledge IIT Hyderabad and CDAC for Computational facilities. Authors would like to thank Dr G S Vaitheeswaran, University of Hyderabad for fruitful discussion. The author VK would like to acknowledge Prof. Brendan Kennedy, University of Sydney for fruitful discussion and critical reading of the manuscript. The author AB acknowledge DST-INSPIRE for fellowship. VK would like to acknowledge CSIR with reference number 03(1433)/18/EMR-II for funding.

Data availability statement

The data that support the findings of this study are available upon reasonable request from the authors.

References

- [1] Gao H, Venderbos J W F, Kim Y and Rappe A M 2019 *Annu. Rev. Mater. Res.* **49** 53–83
- [2] Liu Z K et al 2016 *Nat. Commun.* **7** 12924
- [3] Chiu C-K, Teo J C, Schnyder A P and Ryu S 2016 *Rev. Mod. Phys.* **88** 035005
- [4] Yang S A 2016 *Spin* **6** 1640003
- [5] Bansil A, Lin H and Das T 2016 *Rev. Mod. Phys.* **88** 021004
- [6] Dai X 2016 *Nat. Phys.* **12** 727
- [7] Chen Y, Lu Y M and Kee H 2015 *Nat. Commun.* **6** 6593
- [8] Muechler L, Alexandradinata A, Neupert T and Car R 2016 *Phys. Rev. X* **6** 041069
- [9] Liu Z K et al 2014 *Science* **343** 864–7
- [10] Liu Z K et al 2014 *Nat. Mater.* **13** 677–81
- [11] Xu S-Y et al 2015 *Science* **349** 613–7
- [12] Lv B Q et al 2015 *Phys. Rev. X* **5** 031013
- [13] Yang L X et al 2015 *Nat. Phys.* **11** 728–32
- [14] Novoselov K S, Geim A K, Morozov S V, Jiang D, Zhang Y, Dubonos S V, Grigorieva I V and Firsov A A 2004 *Science* **306** 666
- [15] Zhang Y, Tan Y-W, Stormer H L and Kim P 2005 *Nature* **438** 201
- [16] Wang B, Gao H, Lu Q, Xie W, Ge Y, Zhao Y H, Zhang K and Liu Y 2018 *Phys. Rev. B* **98** 115164
- [17] Fang C, Weng H, Dai X and Fang Z 2016 *Chin. Phys. B* **25** 117106
- [18] Zou J, He Z and Xu G 2019 *npj Comput. Mater.* **5** 96
- [19] Fu P H, Liu J F and Wu J 2020 *Phys. Rev. B* **102** 075430
- [20] Burkov A, Hook M and Balents L 2011 *Phys. Rev. B* **84** 235126
- [21] Fang C, Chen Y, Kee H-Y and Fu L 2015 *Phys. Rev. B* **92** 081201
- [22] Kim Y, Wieder B J, Kane C L and Rappe A M 2015 *Phys. Rev. Lett.* **115** 036806
- [23] Yu R, Weng H, Fang Z, Dai X and Hu X 2015 *Phys. Rev. Lett.* **115** 036807
- [24] Bian G et al 2016 *Nat. Commun.* **7** 10556
- [25] Duan W, Yang C, Ma Z, Zhu Y and Zhang C 2019 *Phys. Rev. B* **99** 045124
- [26] Wan X, Turner A M, Vishwanath A and Savrasov S Y 2011 *Phys. Rev. B* **83** 205101
- [27] Xu G, Weng H, Wang Z, Dai X and Fang Z 2011 *Phys. Rev. Lett.* **107** 186806
- [28] Tang P, Zhou Q, Xu G and Zhang S-C 2016 *Nat. Phys.* **12** 1100–4
- [29] Wang Z, Vergniory M G, Kushwaha S, Hirschberger M M, Chulkov E V, Ernst A A, Ong N P, Cava R J and Bernevig B A 2016 *Phys. Rev. Lett.* **117** 236401
- [30] Hirschberger M, Kushwaha S, Wang Z, Gibson Q, Liang S, Belvin C A, Bernevig B A, Cava R J and Ong N P 2016 *Nat. Mater.* **15** 1161
- [31] Wang X 2008 *Phys. Rev. Lett.* **100** 156404
- [32] Zhang R-W, Zhang Z, Liu C-C and Yao Y 2020 *Phys. Rev. Lett.* **124** 016402
- [33] Chen J Y, Li X X, Zhou W Z, Yang J L, Ouyang F P and Xiong X 2019 *Adv. Electron. Mater.* **6** 1900490
- [34] Sun Q and Kioussis N 2019 *Nanoscale* **11** 6101
- [35] Massa W and Steiner M 1980 *J. Solid State Chem.* **32** 137–43
- [36] Babel D, Wall F and Heger G 1974 *Z. Naturforsch. B* **29** 139
- [37] Brosset C 1937 *Z. Anorg. Allg. Chem.* **235** 139
- [38] Brosset C 1938 *Z. Anorg. Allg. Chem.* **239** 301
- [39] Morón M C, Palacio F, Clark S M and Paduan-Filho A 1995 *Phys. Rev. B* **51** 8660
- [40] Massa W, Molinier M and Pebler J 1995 *J. Fluorine Chem.* **72** 171–6
- [41] Aguado F, Rodriguez F and Nunez P 2007 *Phys. Rev. B* **76** 094417
- [42] Blöchl P E 1994 *Phys. Rev. B* **50** 17953
- [43] Kresse G and Joubert D 1999 *Phys. Rev. B* **59** 1758
- [44] Kresse G and Furthmüller J 1996 *Phys. Rev. B* **54** 11169
- [45] Perdew J P, Burke K and Ernzerhof M 1996 *Phys. Rev. Lett.* **77** 3865–8
- [46] Dudarev S L, Botton G A, Savrasov S Y, Humphreys C J and Sutton A P 1998 *Phys. Rev. B* **57** 1505
- [47] Madsena G K H, Carrete J and Verstraete M J 2018 *Comput. Phys. Commun.* **231** 140–45
- [48] Marzari N, Mostofi A A, Yates J R, Souza I and Vanderbilt D 2012 *Rev. Mod. Phys.* **84** 1419
- [49] QuanSheng W, ShengNan Z, Hai-Feng S, Matthias T and Soluyanov Alexey A 2018 *Comput. Phys. Commun.* **224** 405–16
- [50] Sancho M P L, Sancho J M L and Rubio J 1985 *J. Phys. F: Met. Phys.* **15** 851
- [51] Coey J M D, Venkatesan M and Fitzgerald C B 2005 *Nat. Mater.* **4** 173–9
- [52] Anderson P W 1950 *Phys. Rev.* **79** 350
- [53] Goodenough J B 1955 *Phys. Rev.* **100** 564
- [54] Kanamori J 1958 *J. Phys. Chem. Solids* **10** 87

- [54] Anderson P W 1963 *Magnetism* ed G T Rado and H Suhl (New York: Academic) p 25
- [55] Das H, Waghmare U V, Dasgupta T S and Sarma D D 2008 *Phys. Rev. Lett.* **100** 186402
- [56] Janisch R and Spaldin N A 2006 *Phys. Rev. B* **73** 035201
- [57] Li X *et al* 2014 *Sci. Rep.* **4** 5497
- [58] Zhang S N, Wu Q S, Liu Y and Yazyev O V 2019 *Phys. Rev. B* **99** 035142
- [59] Hu L, Kang L, Yang J, Huang B and Liu F 2018 *Nanoscale* **10** 22231–6
- [60] Guo P J, Yang H C, Zhang B J, Liu K and Lu Z Y 2016 *Phys. Rev. B* **93** 235142
- [61] Zhang J F, Guo P J, Gao M, Liu K and Lu Z Y 2020 *Phys. Rev. B* **101** 155139
- [62] Zhang H, Huang H, Haule K and Vanderbilt D 2014 *Phys. Rev. B* **90** 165143
- [63] He T, Zhang X, Meng W, Jin L, Dai X and Liu G 2019 *J. Mater. Chem. C* **7** 12657
- [64] Yang M *et al* 2020 *Phys. Rev. Mater.* **4** 094203
- [65] Jin Y J, Wang R, Chen Z J, Zhao J Z, Zhao Y J and Xu H 2017 *Phys. Rev. B* **96** 201102(R)
- [66] Yang S-Y, Yang H, Derunova E, Parkin S S P, Yan B and Ali M N 2018 *Adv. Phys. X* **3** 1414631
- [67] Ariel V and Natan A 2013 Electron effective mass in graphene *Int. Conf. on Electromagnetics in Advanced Applications*
- [68] Borisenko S *et al* 2014 *Phys. Rev. Lett.* **113** 027603
- [69] Neupane M *et al* 2014 *Nat. Commun.* **05** 3786
- [70] Lang M *et al* 2012 *ACS Nano* **6** 295–302